Title

Decoupling of plate-asthenosphere motion caused by non-linear viscosity during slab folding in the transition zone

Authors

Billen, Magali I
Arredondo, Katrina M

Publication Date

2018-08-01

DOI

10.1016/j.pepi.2018.04.011

Peer reviewed

Decoupling of Plate-Asthenosphere Motion Caused by Non-linear Viscosity During Slab Folding in the Transition Zone

Magali I. Billen[a], Katrina M. Arredondo[a]

[a]*Department of Earth and Planetary Sciences, U. C. Davis*

Abstract

Although most present-day subduction zones are in trench retreat, plate reconstructions and geological observations show that individual margins experience episodes of advancing, retreating or stationary trench motion with time-variable subduction rates. However, most laboratory and numerical simulations predict steady plate velocities and sustained trench retreat unless the slab experiences folding in the transition zone. Using 2D dynamical models of subduction with a mobile trench and overriding plate, we find that rapid sinking of the slab during folding causes a reduction in asthenosphere viscosity through the non-linear rheology, which allows the overriding plate to move in the opposite direction of the asthenosphere. This decoupling of the direction of plate and asthenosphere flow allows for episodes of rapid trench advance after each slab folding event. By analyzing the interaction between slab deformation (sinking direction and speed), stress-induced changes in asthenosphere viscosity, asthenosphere flow and plate motions, we show that there are three modes of slab-flow-plate interaction: 1) coupled trench retreat during rapid vertical sinking, 2) coupled trench advance during prograde sinking of the slab, and 3) decoupled, rapid trench advance during folding with prograde motion of the shallow slab and retrograde motion of the deep slab. These results show that non-linear viscosity plays an important role in determining the force balance controlling trench motion and conversely that trench motion can be used as a constraint on the asthenosphere viscosity underlying the overriding plate. In addition, cooling by several hundreds of degrees during episodes of fast subduction could lead to a reduction in slab dehydration and fluid-induced melting in the mantle wedge. Such cold episodes would also likely lead to time-variability in the water content and related geochemical tracers in erupted lavas, as well as the amount of water being transported by slabs into the deep mantle.

Keywords: slab deformation, phase transitions, plate-mantle coupling, rheology, slab thermal structure, mantle wedge thermal structure

1. Introduction

The motion of tectonic plates at the Earth's surface is the most direct observation of large-scale mantle flow reflecting the time-dependent balance of driving and resisting forces acting on the base of the plates and through slab-pull and ridge push (Forsyth and Uyeda, 1975; Lithgow-Bertelloni and Richards, 1998; Conrad and Lithgow-Bertelloni, 2002; Gérault et al., 2012). A recent analysis of present-day trench motion using different reference frames concludes that 62–78% of trenches are in retreat, with median trench velocity of 0.9–1.3 cm/yr (retreating), and faster retreat only observed near slab edges (Schellart et al., 2008). In about 80% of subduction zones, subducting plate motion accounts for more than 50% of net convergence (Schellart et al., 2011). Plate tectonic reconstructions of past plate motion also show that individual trenches experience both advancing and retreating motion, although this is hard to constrain further back in time (Sdrolias and Müller, 2006).

Subduction zone force-balance analysis attempts to account for how each of the forces acting on the subducting plate, overriding plate, slab, and across the plate boundary interface, result in the observed plate motions (Forsyth and Uyeda, 1975). There have been various iterations of force-balance models, each making different assumptions or simplifications in an attempt to elucidate the first-order balance of forces controlling trench motion (Schellart, 2004; Heuret and Lallemand, 2005; Stegman et al., 2006; Lallemand et al., 2008; Billen, 2008; Capitanio, 2013; Holt and Becker, 2017). In a more sophisticated approach, semi-analytic flow solutions accounting for the forces due to poloidal (corner-flow) and torroidal flow induced by the sinking slab are combined to predict trench motions (Royden and Husson, 2006; Capitanio et al., 2007; van Dinther et al., 2010). In all of these analysis, when the overriding plate is included, it is assumed that the plate and underlying asthenosphere move in the same direction. If the asthenosphere moves faster than the plate, then is exerts a driving force on the plate helping to drag it forward, whereas if the asthenosphere moves slower it exerts a resisting force.

While most force-balance analysis assume a steady-state slab geometry, the observed shapes of subducting slabs (e.g., van der Hilst et al., 1997; Ritsema et al., 2004) are due to the time-dependent variation in both driving and resisting forces and resulting changes in plate and trench motions. For example, trench retreat combined with increased resistance to sinking into the lower mantle is thought to form sub-horizontal slabs just above, on, or just below the upper-lower mantle boundary at 660 km (Fukao et al., 2009). Whereas, broadening of slabs in the lower mantle is thought to be caused by folding or buckling of the slab as it encounters increased resistance to sinking into the lower mantle (Ribe et al., 2007). Such buckling has been shown to depend on the strength contrast between the slab and the surrounding mantle and the viscosity contrast (and/or resistance due to phase transitions) across the upper-lower mantle boundary (Ribe, 2010; Stegman et al., 2010; Lee and King, 2011).

Geodynamic models of subduction show that strong trench retreat is promoted by stiff and less dense slabs (Funiciello et al., 2008; Garel et al., 2014; Agrusta et al., 2017), shorter along-strike trench length (Stegman et al., 2006; Schellart et al., 2007; Stegman et al., 2010), proximity to a slab edge (Schellart et al., 2011) and thinner and/or more buoyant overriding plates (Holt et al., 2015). A synthesis of results from analogue models found that both weak ($\eta_{slab}/\eta_{mantle} < 10^2 - 10^3$) *or* stiff ($\eta_{slab}/\eta_{mantle} > 10^4$) *and* less-dense slabs exhibit trench retreat, with intermediate slab stiffness generating either slab folding or trench advance (Schellart, 2008b). Similarly, a comprehensive study using 3D numerical models (but not including the lower mantle or an overriding plate) and linear visco-plastic rheology showed that dense and weak or less dense and stiff slabs exhibited trench retreat with or without folding, respectively, while dense and stiffer slabs exhibited slab folding and trench advance (Stegman et al., 2010). However, it has also been shown that non-linear viscosity, which increases $\eta_{slab}/\eta_{mantle}$ by weakening the mantle, promotes trench advance

(Holt and Becker, 2017) consistent with the results of simulations exhibiting slower rates of trench retreat (Quinteros et al., 2010; Garel et al., 2014).

In addition to subduction geometry and rheology, phase transitions also affect slab dynamics and surface plate motion (Christensen, 1996; Cížková et al., 2007; Cížková and Bina, 2013; Agrusta et al., 2017; Yoshida, 2017). In simulations similar to Quinteros et al. (2010) and (Garel et al., 2014), but including a strong negative Clapeyron slope for the phase transition at 660 km, strong trench retreat occurs, but with time-variable subduction rates due to localized slab buckling in the transition zone (Cížková and Bina, 2013). In contrast to these models, a study by Arredondo and Billen (2017) found that when using a more complete compositionally-dependent phase transition (CDPT) model, non-linear rheology and a deep model domain (bottom at the core-mantle boundary) trench motion was primarily in advance, even with episodic slab folding in the transition zone. However, the study by Arredondo and Billen (2017) was focused on the effect of the new CDPT model and the role of the shear zone viscosity and plastic yielding on slab behavior and did not consider how other aspects of the model affected slab deformation and trench motion. These divergent model behaviors found in similar studies illustrates the complex feedback that occurs between different choices of model parameters (e.g., phase transitions, type of rheology) and model design (e.g., 2D vs. 3D, box depth), making it challenging to constrain the balance of forces controlling plate and trench motion.

The thermal structure of the shallow slab and mantle wedge can also provide a further constraint on geodynamic models of subduction because the mantle wedge must remain hot enough to generate magmas that feed the volcanic arc (Elkins-Tanton et al., 2001; Kelemen et al., 2003; Cagnioncle et al., 2007; England and Katz, 2010). This constraint is violated in most global models of subduction simply because the resolution necessary to accurately model the mantle wedge is not usually computationally feasible although this is changing (see Stadler et al., 2010; Alisic et al., 2010). However, most subduction modeling studies also do not explicitly consider this constraint (however, see Arcay, 2017) and sometimes end up with a broad, deep, cold mantle wedge corner (Cížková and Bina, 2013; Garel et al., 2014; Agrusta et al., 2017). The broad, thick and higher viscosity region that develops above the slab in these models is also likely to affect how the slab deforms by preventing the shallow slab dip from changing and creating a large positive pressure above the slab (pushing it backwards).

Here we build on the growing understanding of the link between slab deformation and plate motions from previous studies in an effort to disentangle the various model design and parameter choices that determine slab, flow and plate interaction. Here, we first build on the Arredondo and Billen (2017) study by varying the overriding plate structure (age, compositional density, and a spreading ridge) and show that while these changes do produce more trench retreat, the model parameters still do not produce steady trench retreat as found in many other models. Instead, we present new analysis showing that non-linear viscosity controls the time-dependent balance of forces on the overriding plate and trench through stress-induced reduction of the asthenosphere viscosity (as low as 10^{18} Pa s). The low viscosity allows for decoupling the direction of flow in the asthenosphere from that in the overriding plate. More specifically, by analyzing the interaction between slab deformation (sinking direction and speed), stress-induced changes in asthenosphere viscosity, and asthenosphere flow and plate motions, we show that there are both periods of coupled motion of the overriding plate and underlying asthenosphere in retreat (mode 1) or advance (mode 2), and there are periods of decoupled motion during which the overriding plate advances while the underlying asthenosphere is pulled toward the slab (mode 3). In addition, we show how the resulting time-variable subduction leads to changes in the thermal structure of the slab and mantle wedge, the resulting effect on slab dynamics, and how this compares to the steady-state thermal structure resulting from kinematic-slab wedge-flow thermal models (Peacock and Wang, 1999; van Keken et al., 2002; Currie et al., 2004; Wada et al., 2008; Syracuse et al., 2010).

2. Methods

We model the time-evolution of slab deformation and thermal structure, in a two-dimensional equatorial slice of a sphere, using the finite element code CitcomS (Zhong et al., 2000; McNamara and Zhong, 2004; Tan et al., 2006). CitcomS solves the conservation equations for mass, momentum and energy using the extended Boussinesq approximation, which assumes incompressibility but includes an initial adiabatic gradient, shear heating and latent heat from phase transitions (Christensen and Yuen, 1985; Ita and King, 1994). The full model domain is 61° in longitude and 2890 km in depth with a minimum element size of 1.5 km x 2.5 km in a 1000 km wide by 170 km deep region centered at 35° (Fig. 1a). The element size then gradually increases with depth and longitudinal distance reaching a maximum size of 8.3 km x 10 km below 1100 km. There are free-slip boundary conditions on all the domain boundaries (Fig. 1a).

Initial Temperature and Composition. The top and bottom surface are isothermal (0°C; 2075°C) and there is an initial adiabatic gradient of 0.25 K/km starting at 190 km depth. The sidewalls are insulating. The subducting and overriding plates are defined thermally using a half-space cooling model and the age of the plate: for the subducting plate the initial age increases from a ridge at 0° longitude to either 40 my or 80 my using a constant spreading rate. The age of the overriding plate is constant (either 20 or 40 my), except in some models in which a spreading ridge is added at the model boundary at 61° (see Table 1). The proto-slab is created by first running the model with kinematic surface boundary conditions (5 cm/yr on the subducting plate) until the tip of the slab reaches 200 km depth (Fig. 1a, b). The density anomaly of the slab depends on the minimum temperature of the slab, which varies with a maximum difference in the range of 33 – 46 kg/m^3 for a temperature anomaly of 500–700°C.

In addition to the temperature, the plates are also defined by compositional layers that are tracked using tracer particles (Fig. 1b): a 7.5 km basaltic crust (3000 kg/m^3) overlying a 27.5 km harzburgite (3235 kg/m^3) layer, with the remaining mantle having the composition of pyrolite (3300 kg/m^3). In some models these layers are omitted on the overriding plate to test the effect of compositional buoyancy on plate motion. Basalt is modeled as transitioning to eclogite (3540 kg/m^3) starting at 700°C for pressures above 15 kbar and ending at 850°C (Arrial and Billen, 2013; Arredondo and Billen, 2016).

Rheology. The rheology is the same as that used in previous studies (Billen and Hirth, 2007; Arredondo and Billen, 2017). The upper mantle (pyrolite, harzburgite, eclogite) are modeled with a composite viscosity using the flow-laws

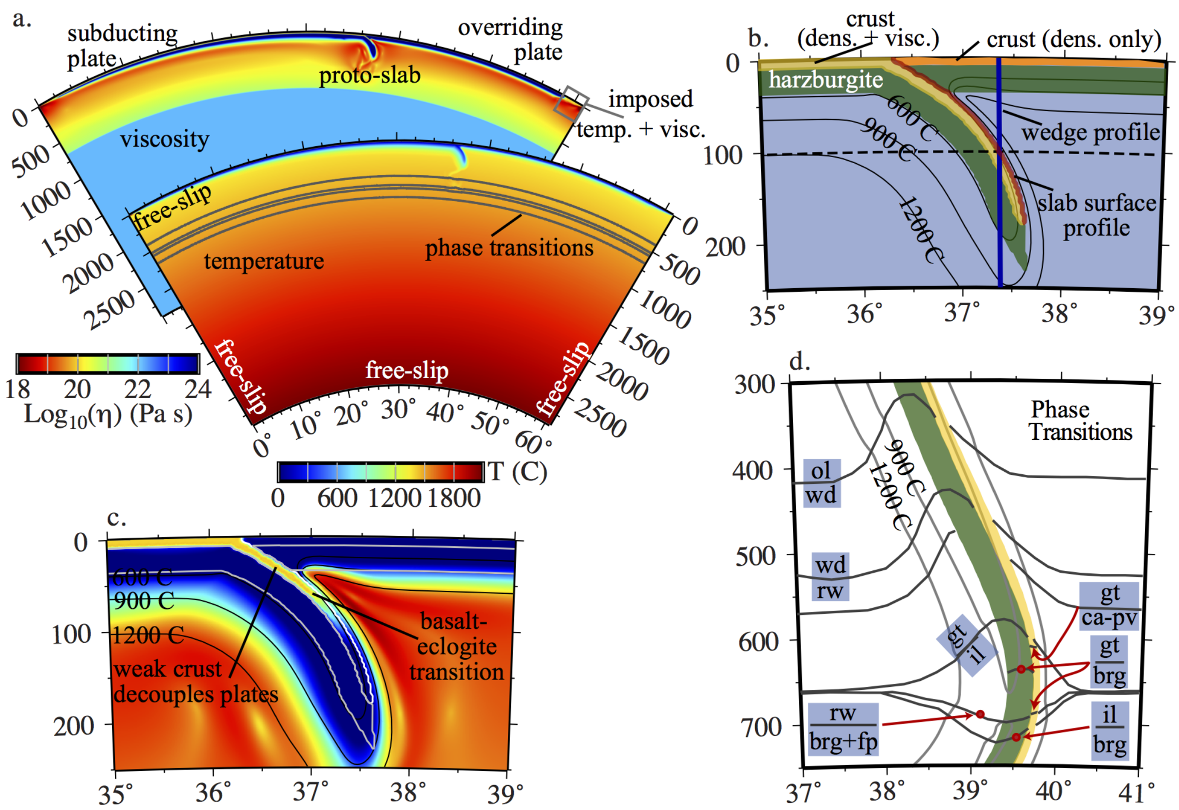

Figure 1: Model Design. a) Full Model domain showing initial viscosity and temperature structure, phase transitions and boundary conditions. Note 500 km wide box on trailing edge of overriding plate: the temperature and viscosity are reset in the box to allow for a mobile overriding plate and preventing formation of a subduction zone or maintaining the imposed mid-ocean ridge. b) Compositional layers and profile locations used to analyze the evolution of the temperature structure. Yellow layer: oceanic crust (basalt or eclogite density, fixed viscosity). Green layer: harzburgite with an olivine flow-law. Orange layer: oceanic crust (basalt density only). Light blue background: pyrolite composition with olivine flow law. Red contour: the slab surface profile follows the top of the crustal layer. Blue profile: the vertical wedge profile is located at the longitude where the slab-surface crosses a depth of 100 km. Note that because the slab and trench are free to move, the absolute location of the profiles change with time. c) Zoom-in on subduction plate boundary showing the viscosity structure for the proto-slab. The subducting and overriding plate are decoupled by a weak crustal layer with basalt-eclogite composition. Black contours are temperature. White contours outline the crust and harzburgite layers (shown in yellow and green in parts C and D). d) Zoom-in on the transition zone showing the compositionally-dependent phase transition boundaries across a sinking slab (snap-shot is from model 4 at 46.0 my). Yellow/green layers are crust/harzburgite composition.

for diffusion and dislocation creep in olivine (Hirth and Kohlstedt, 2003) and a depth dependent yield stress reaching a maximum yield stress of 1000 MPa at 80 km. The background, upper mantle viscosity is 10^{20} Pa s at 250 km depth for a strain-rate of 10^{-15} $s^{-}1$ and increases with depth. The maximum viscosity for the basalt layer is 10^{20}Pa s, which allows the subducting plate to slide past the overriding plate (Fig. 1c). The viscosity of this layer smoothly transitions to the olivine viscosity as the basalt composition transitions to eclogite. The lower mantle is modeled using the diffusion-creep flow law for olivine, with a large intrinsic grain size, to assign a background viscosity of 10^{22} Pa s. The full range of viscosity allowed in the models is 10^{18}–10^{24} Pa s and occurs between the mantle surrounding the slab, mantle wedge, or asthenosphere and the cold interior of the slab or lithosphere, respectively.

For models without a spreading ridge on the overriding plate, we impose a 500-km wide region of low viscosity at the domain boundary to allow the overriding plate to freely move toward or away from the model edge. The temperature within this region is also held fixed to prevent the formation of a downwelling during times of trench advance or a ridge during trench retreat (unless a ridge is explicitly included in the model). Note that because the low viscosity crustal layer is being tracked by tracer particles, the subduction location is free to move in response to the slab dynamics and tractions acting on the bottom of the plates.

Phase Transitions. A compositionally-dependent phase transition (CDPT) model tracks the proportions of the olivine, pyroxene and garnet minerals in each composition and the phase transitions for these minerals (Fig. 1d): for specific model parameters and complete references see Arredondo and Billen (2016) and Arredondo and Billen (2017). For the olivine component, the phase transitions include olivine → wadsleyite (410 km), wadsleyite → ringwoodite (520 km), and ringwoodite → bridgmantite+ferropericlase (660 km). For the pyroxene component, there is a non-temperature dependent dissolution to garnet starting at about 300 km depth that we do not include because it does not affect the density anomaly between the slab and the surrounding mantle. Calcium-perovskite starts to form at around 560 km depth from exsolution of calcium-rich garnet and dissolution of clinopyroxene. This transition occurs deeper in the eclogite layer (665 km) and does not occur in harzburgite. Majoritic garnet either transitions directly to bridgmanite, or in cold regions, first transitions to ilmenite above 660 km and then ilmenite transitions to bridgmanite below 660 km.

Compared to models assuming a 100% olivine composition, the single phase transition at 660 km occurs as a series of transitions with both positive and negative clapeyron slopes, which act to decrease the overall resistance to subduction at the base of the transition zone. And, unlike previous models considering only the phase transitions at 410 km and 660 km, the additional phase transitions in the mid-transition zone add to the overall negative buoyancy of the slab (Arredondo and Billen, 2017).

3. Results

We first present the dynamical behavior of the models describing the relationship between slab dynamics, trench and plate motion and the model parameters (see statistics in Table 1). Second, we present the effect of time-variable slab dynamics on slab and wedge thermal structure. Movies (S1–S7) of the simulations are available in the Supplemental Information.

3.1. Slab Folding, Trench and Plate Motions

As has been shown in the previous work discussed in the introduction, we find that the resistance to sinking at 660 km from a combination of the increase in viscosity and the phase transitions leads to episodic folding of the slab in the transition zone (models 1–6; Fig. 2b–d and movies in supplemental information). In contrast the slab in an identical

Table 1: Summary of Variable Model Parameters & Plate Motion Results

Model	OP/SP Age (My)	Slab Dyn. -	Model Duration (my)	Trench Motion (a, r, s) %	Trench. Vel. +max, -max (cm,/yr)	OP Vel. med, +max, -max (cm/yr)	SP Vel. med, maxlt (cm/yr)
No Overriding Plate Compositional Buoyancy							
1	20/80	f	49.5	76.1, 19.4, 4.5	3.4, -1.3	0.7, 3.1, -1.5	4.6, 11.1
1c	20/80	b	19.0	η_{cr} = 10^{21} Pa s, slab breaks off			
2	40/80	f	40.6	47.9, 42.3, 9.8	4.2, -2.3	1.4, 4.6, -0.8	3.7, 15.5
With Overriding Plate Compositional Buoyancy							
3	20/80	f	61.6	41.3, 49.6, 9.0	1.6, -0.5	0.1, 1.8, -0.4	2.4, 6.2
3c	20/80	b	18.9	η_{cr} = 10^{21} Pa s, slab breaks off			
With OP Buoyancy and OP Spreading Ridge							
4	20/80	f	65.2	35.8, 60.2, 4.1	2.6, -1.3	0.0, 2.4, -1.6	4.2, 9.7
5	20/40	f	44.8	49.5, 40.1, 10.4	2.3, -1.4	0.3, 2.2, -1.2	5.7, 10.3
6, η_{min}	20/80	f	62.1	9.5, 86.3, 3.4	0.5, -1.1	-0.3, 0.1, -1.1	2.6, 4.7
7, no PT	20/80	v	43.3	14.0, 75.0, 11.0	0.3, -1.1	-0.1, 0.7, -0.6	2.7, 5.0
7c, no PT	20/80	b	19.1	η_{cr} = 10^{21} Pa s, slab breaks off			

Plate/trench velocities are positive in the direction of increasing longitude. Stationary is defined as a trench velocity less than ±0.1 cm/yr. OP/SP: overriding plate/subducting plate. Slab Dynamics: folding (f), slab breakoff (b), vertical sinking (v). a/r/s: percentage of model run time that trench motion is in *a*dvance, *r*etreat, or *s*tationary. Plate/trench velocity ranges are determined starting 3 my after the peak SP velocity (maxtz) that occurs as the slab first enters the transition zone: med – median velocity, maxlt – maximum long term, +max – maximum positive velocity, -max – maximum negative velocity. no PT: no phase transitions were included in these models. The slab breaks-off in models 1c, 3c, and 7c (with a higher crustal viscosity) at the time listed as model duration: no further analysis is done for these models.

model with no phase transitions sinks directly into the mantle without folding showing that the viscosity jump of 100x is not sufficient to cause folding given the strength of the slab (model 7, maximum yield strength of 1 GPa; Fig. 2a).

Slab folding leads to episodic motion of the trench and plates in which velocity increases and then decreases during each folding event (Fig. 3). However, unlike several previous studies we find that there is no underlying steady trench retreat. The subducting plate velocity is primarily controlled by the minimum crustal viscosity and the relative viscosity contrast between the slab and the surrounding mantle, the latter of which varies because the minimum viscosity of the upper mantle changes in response to the changing negative buoyancy of the slab (including the added density due to phase transitions). The crustal viscosity value of 10^{20} Pa s leads to a subducting plate velocity range of 2–15 cm/yr after the initial decent of the slab through the upper mantle in agreement with observed rates of plate motions (Table 1). However, if shear zone viscosity is increased by a factor of 5–10 the slab breaks off because there is too much viscous resistance at the trench compared to the growing stress within the slab as it crosses the phase boundaries in the transition zone (models 1c, 3c, 7c).

The folding of the slabs can be characterized by the fold frequency (how often a fold occurs) and the amplitude of the fold (the horizontal distance between inflection points). A younger, mechanically thinner slab has a higher frequency (25 my) compared to a mechanically stronger slab (50 my), but both have similar fold amplitudes (450 km; Fig. 2b vs. c; model 5 versus model 4). The folding behavior is also affected by limiting the minimum mantle viscosity to 5×10^{19} Pa s in two ways (Fig. 2d). First, the average sinking rate decreases (Table 1) causing the fold frequency also to decrease. Second, the amplitude of the folding is smaller (250 km) due to the larger resistance to horizontal motion of the slab through the upper mantle.

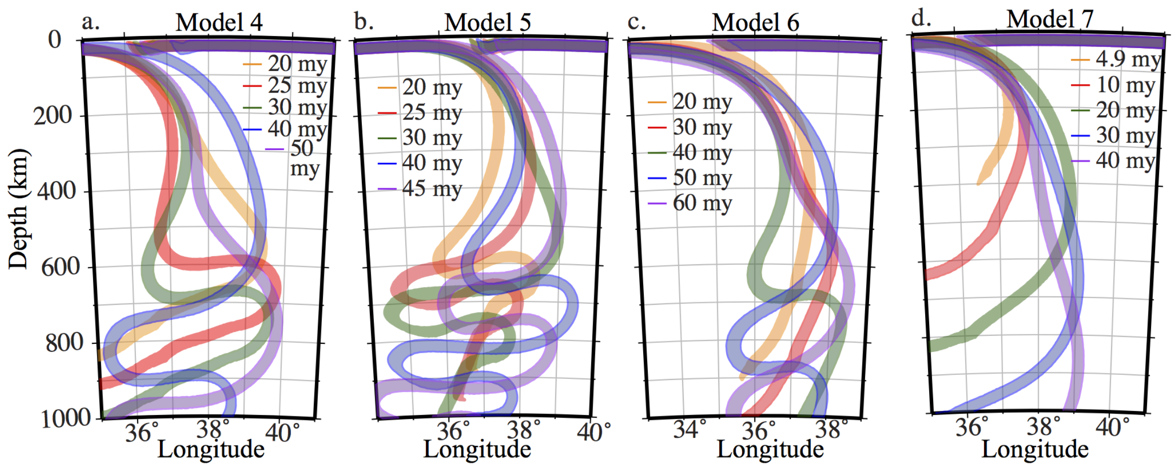

Figure 2: Comparison of slab dynamics in models with different phase change models. a) Model 4 with an older subducting plate (80 my) has less frequent folds than model 5. b) Model 5 with a young subducting plate (40 my) exhibits multiple folding events. c) Model 6 with a minimum viscosity cut-off of 5×10^{19} Pa s has smaller folding amplitudes and less frequent folding. d) Model 7 with no phase changes: slab sinks directly into the lower mantle and there is little time-dependent behavior.

To understand what might lead to the oscillatory-dominated trench motion, we explored several model parameters that had been previously suggested to control trench motion. First, we compared the effect of overriding plate thermal density (model 1 and 2) and found that following strong trench advance at the start of the simulation as the slab rapidly sinks into the transition zone, the plate motions are similar until about 35 my (Fig. 3). At about 35 my an unusual arc rifting event occurs in model 2 (see Billen, 2017) preventing further comparison of the models. During each folding event the trench moves rapidly toward the overriding plate (advance). However, by adding compositional buoyancy to the overriding plate there is a shift from 76% trench advance (model 1) to only 41% (model 3). The trench motion is also slower overall and spends almost 9% of the time stationary (i.e., velocity less than ±0.1 cm/yr; see Table 1).

Therefore, we conclude that overriding plate buoyancy does affect trench mobility by equalizing the isostatic pressure gradient between the overriding and subducting plates.

Next we add a spreading ridge to the overriding plate. Most numerical models that include temperature have included a spreading ridge on the overriding plate (Čížková and Bina, 2013; Garel et al., 2014; Agrusta et al., 2017), while mechanical models with prescribed density also include a ridge-push force because normal density material fills in behind the subducting slab (Stegman et al., 2010; Holt and Becker, 2017). However, the effect of this ridge-push force on trench motion has not been explicitly test. In addition, an analytical force-balance calculation has attributed trench advance to an unbalanced force from ridge push on the subducting plate (Capitanio, 2013). Therefore, the hypothesis that we are testing is that by only including a ridge on the subducting plate, there is a ridge-push force on the subducting plate side that is unbalanced causing the trench to always advance. By adding a spreading ridge on the overriding plate side, then the ridge push forces can be balanced. Comparison of models 3 and 4 show that adding the ridge push force only slightly decreases the amount of time spent in trench advance (from 41.3% to 35.8%), but it does decrease the amount of time the trench is stationary and therefore the trench is in retreat for 60% of the time (Table 1; Fig. 3). However, trench advance rates are still about twice as fast the trench retreat rates and therefore there is almost no net motion of the trench.

Other studies have concluded that trench retreat occurs for both weaker slabs or stiffer and less dense slabs (Funiciello et al., 2008; Schellart, 2008b; Ribe, 2010): because we use temperature-dependent rheology it is not straightforward to make the slab less dense while also making it stiffer. In addition, while oceanic floor older than 80 my is commonly subducted, the observation of flattening of the age-subsidence curve suggest that oceanic lithosphere does not continue to thicken for ages greater than 80 my (Stein and Stein, 1992). However, we can test the effect of decreasing the stiffness of the slab by using a younger subducting plate. Here we test this by comparing the trench motion for an old subducting plate (80 my; model 4) to that for a young subducting plate (40 my; model 5). We find that because the younger slab folds more frequently, this actually leads to more time in trench advance or with a stationary trench.

Finally, while most previous models had not explicitly considered the role of asthenosphere viscosity on trench motion, a recent study showed that non-linear rheology could reduce trench retreat (Holt and Becker, 2017). In addition, other models with similar set-up and rheology, but with more trench retreat use a larger minimum viscosity cut-off of 10^{19} Pa s (Čížková and Bina, 2013) or 10^{20} Pa s (Garel et al., 2014). To test this effect in our model set-up, we changed the minimum viscosity cut-off in the model from 10^{18} Pa s to 5×10^{19} Pa s (model 6). Increasing the minimum viscosity decreases the plate speeds from a median of 5.7 cm/yr to only 2.6 cm/yr and from a maximum of 10.3 cm/yr to only 4.7 cm/yr. It also leads to more trench retreat (70%): in particular there is a fast pulse of trench retreat occurring at the start of the model as the slab sinks rapidly into the transition zone. However, after this initial phase, the trench retreats very slowly and the overall slab location remains relatively fixed with the folding event of the slab at 35–45 my overlapping the location of the slab at 10 my. Therefore, starting at about 35 my, trench retreat is mainly caused by a slow decrease in the shallow slab dip (increase in radius of curvature; see Fig. 7B) and, from

50–60 my, the growth of the accretionary prism.

One important remaining difference between our models and previous models is that the slabs sink into the lower mantle, while in other models the slabs do not sink into the lower mantle for various reasons (resistance due to viscosity jump, phase transition or a box boundary at 660 km). This leads to a different structure/geometry for the return flow in mantle. In our models the return flow is primarily broad and deep, while in these other models the return flow is isolated in the upper mantle. This difference in return flow structure may also be an important factor favoring trench retreat.

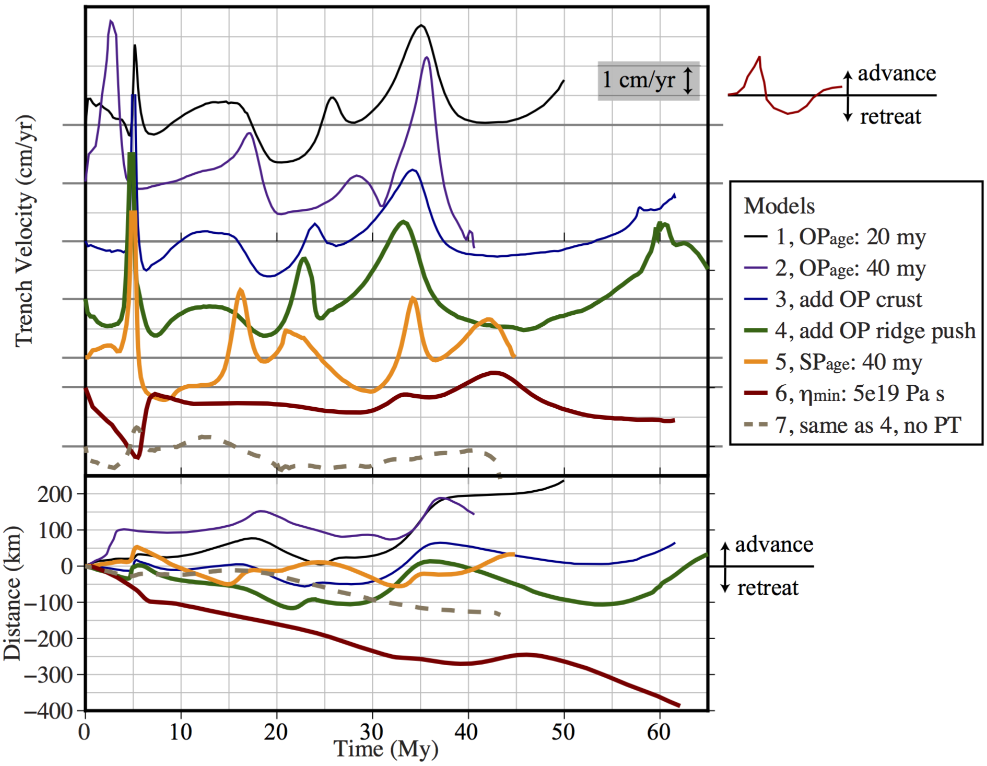

Figure 3: Trench motion. Top: trench velocity as a function of time illustrating the episodic variation of plate motion in response to folding of the slab for models 1–5. Model 7 has no slab folding. Model 6 has slab folding, but smaller corresponding changes in trench motion. Positive velocity is toward the overriding plate (advance). Negative velocity is toward the subducting plate (retreat). Bottom: distance moved by the trench with respect to the starting position. Positive distance is trench advance. Only models 6 and 7 exhibit a net trench retreat.

To further understand what is controlling the motion of the overriding plate and trench in the models, which differs significantly from most previous models, we examined how deformation of the slab and the induced mantle flow is coupled to motion of the overriding plate. In the case of steady sinking of the slab, we would expect that the sinking motion of the slab pulls the shallow surrounding mantle in and pushes the deeper surrounding mantle down and away (Billen, 2001; Gérault et al., 2012). It is also commonly assumed that asthenosphere flow beneath the overriding plate is in the same direction as the plate motion (Forsyth and Uyeda, 1975; Royden and Husson, 2006; Schellart, 2008a;

Capitanio, 2013; Holt and Becker, 2017). In this case, if the asthenosphere is moving faster than the plate then it exerts a driving force on the plate dragging it toward the subduction zone. Whereas if the asthenosphere moves slower it exerts a resisting force slowing the overriding plate motion toward the trench. However, we find that there are times in which the overriding plate and the asthenosphere flow are in opposite directions.

Figure 4 shows snap-shots of the slab evolution with velocity vectors for three of the models (also see Movies S4–S6; Figures S4–S6). Each of the rows in this figure compares the models at a similar state of slab evolution. In the top row, folding of the slab has lead to rapid, near-vertical sinking of the slab, which drives rapid flow of the asthenosphere toward the slab, but the overriding plate is moving away from the trench (except in the model 6 with $\eta_{min} = 5 \times 10^{19}$ Pa s). We refer to this as *decoupled plate motion (mode 3)*, indicating that the *direction of flow* for overriding plate and underlying mantle flow are in opposite directions. In the middle row, the horizontal component of slab motion is directed toward the overriding plate following sinking of a previous fold and this drives asthenosphere and overriding plate motion away from the trench (coupled advance, mode 2). Finally, in the bottom row the slab is shown just before a folding event starts or is starting (model 6): both asthenosphere and overriding plate motion are toward the trench with the asthenosphere dragging (leading) the overriding plate (coupled retreat, mode 1). These snap-shots show that when the slab deformation includes folding, then coupling between mantle flow and the plates can be considerably more complex than expected from models with steady sinking and trench retreat.

The difference in behavior of models 4 and 5 compared to model 6 suggest a link between the non-linear rheology and decoupling of the asthenosphere flow from the overriding plate motion. Figure 5 compares plate motions with the asthenosphere flow and viscosity beneath the overriding plate, and the horizontal component of slab motion as function of depth for models 4–7. The supplemental information includes similar figures for all the models with additional parameters plotted (Figures S1–S7). The supplemental figures show that the subducting plate velocity and the slab velocity are always correlated and very similar in magnitude, and that the vertical component of slab velocity is remarkably constant in depth, although it varies a lot through time. This means that there is strong viscous coupling between the slab and the subducting plate and that the subducting slab must accommodate changes in stresses by horizontal motion. Therefore, a profile of subducting plate speed also shows how the magnitude of slab velocity is changing with time, while the horizontal component of slab velocity shows how the slab is responding to changing stresses. In figure 5 model 4 acts as a reference model, while model 5 shows the effect of changing the mechanical stiffness of the slab (through slab age), model 6 shows the effect of limiting the effect of the non-linear rheology (approximated by limiting the minimum viscosity), and model 7 shows the effect of not including phase transitions.

For models 4–7, we see that there are variations in subducting plate speed (slab sinking rate) with time, but these variations are smaller and occur less often for models 6 and 7. Also, the profiles of overriding plate velocity and trench velocity are very similar, with the small differences mainly being due to accretion of crustal material from the subducting plate. In some cases, the peaks in subducting plate (slab) velocity are matched by a switch to advancing motion of the subducting plate, but not always. The asthenosphere velocity below the overriding plate is sometimes moving with the overriding plate in retreat (mode 1) or advance (mode 2), while at other times it is directed in the

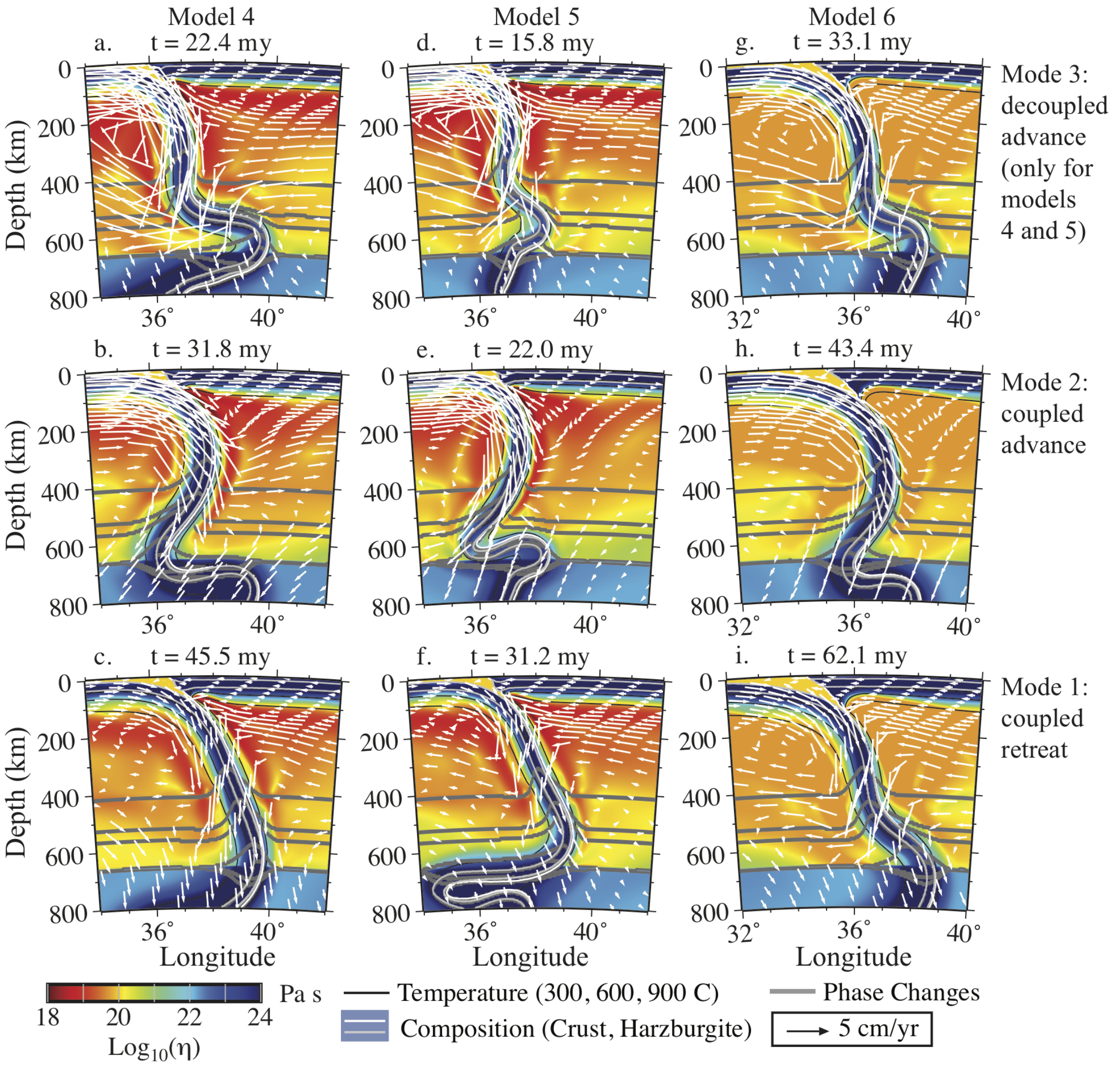

Figure 4: Time-evolution of coupling between slab, mantle and plate motion. a–c) Model 4: with overriding plate buoyancy, a spreading ridge and an old subducting plate (80 my). d–f) Model 5: same as model 4, but with younger subducting plate (40 my). .g–i) Model 6: same as model 4, but with a minimum viscosity cut-off of 5×10^{19} Pa s. Rows compare flow during similar states of slab evolution. Bottom row: mode 1 (coupled retreat) just before or at the start of slab folding both asthenosphere and overriding plate motion are toward the trench. Middle row: mode 2 (coupled advance) slab advance following sinking of a previous fold drives asthenosphere and overriding plate motion away from the slab. Top row: mode 3 (decoupled advance) slab buckling drives rapid asthenospheric flow toward the slab, but the overriding plate is moving in the opposite direction (except for model 6).

opposite direction (mode 3). For model 7 with no phase transitions and no slab folding, only coupled flow occurs (mode 1 and 2), with a short period of advance followed by retreat. The subducting slab also has a larger component of horizontal motion at shallow depth during coupled advance. Similar periods of coupled advance and coupled retreat are seen in models 4–6, and are also correlated with the magnitude and depth extent of horizontal motion of the slab. The fact that coupled advance occurs when there is a large component of positive horizontal (prograde) slab motion indicates that the stiffness of the slab is also an important factor affecting the amount of trench advance in the models. For example, when the slab is mechanically weaker as in model 5, the prograde, horizontal motion of the slab and the advance rate of the overriding plate, are also smaller.

Models 4 and 5 also exhibit short periods of rapid trench advance while the underlying asthenosphere is flowing toward the slab (decoupled advance, mode 3). During this period, we see that three things are happening. First, the subducting plate velocity, and therefore also the slab sinking speed are high. Second, the slab is folding in opposite directions at the top of the slab (positive, prograde) compared to the bottom (negative, retrograde), as can be seen by horizontal slab motion. Third, there is stress-induced weakening of the asthenosphere beneath the overriding plate resulting in viscosity that drop below 10^{19} Pa s. This suggests that the changing buoyancy forces and geometry of the slab results in internal weakening and folding of the slab. Folding of the slab causes rapid sinking and pulls the asthenosphere and mantle toward the folding slab, which has negative (retrograde) horizontal flow at larger depths. However, at shallow depths the slab has positive horizontal motion indicating that there is net subducting-plate and slab motion toward the overriding plate. Finally, because there is stress-induced weakening of the asthenosphere under the overriding plate, the motion of the overriding plate can decouple from the mantle flow being pulled toward the slab.

The important roll of the non-linear viscosity in allowing for this decoupled motion is seen by comparing models 4 and 6. Limiting the minimum viscosity to 5×10^{19} Pa s prevents the decoupled motion from occurring, and the model exhibits net trench retreat. Also, we note that there is also stress-induced weakening in the asthenosphere beneath the subducting plate in models 4 and 5 (see supplemental Figs. S4 and S5). However, this weakening occurs for longer periods of time, not just during the times of decoupled advance, and not just during periods of faster subducting plate and slab motion. Therefore, this analysis supports the conclusion that it is the weakening beneath the overriding plate that is important in controlling the switch from mode 1 or 2 flow to mode 3 flow.

Together these three observations of model behavior during decoupled advance show that the sinking rate of the slab causes changes in asthenosphere viscosity through the non-linear rheology and that this in turn determines whether the asthenosphere and mantle are coupled or can flow in opposite directions. This suggests that when the motion of the overriding plate and asthenosphere are decoupled, the excess prograde horizontal motion of the subducting plate is transferred directly to the overriding plate and can drive trench advance even though the asthenosphere is flowing in the opposite direction. Because the trench advance rate is faster in these periods of decoupled advance, the net trench motion is strongly affected by the short periods of decoupled plate motion. However, when the overriding plate and asthenosphere are coupled, asthenospheric drag on the overriding plate either works against the subducting plate to maintain trench retreat or helps to drag the overriding plate away from the subducting plate creating space for slow trench advance.

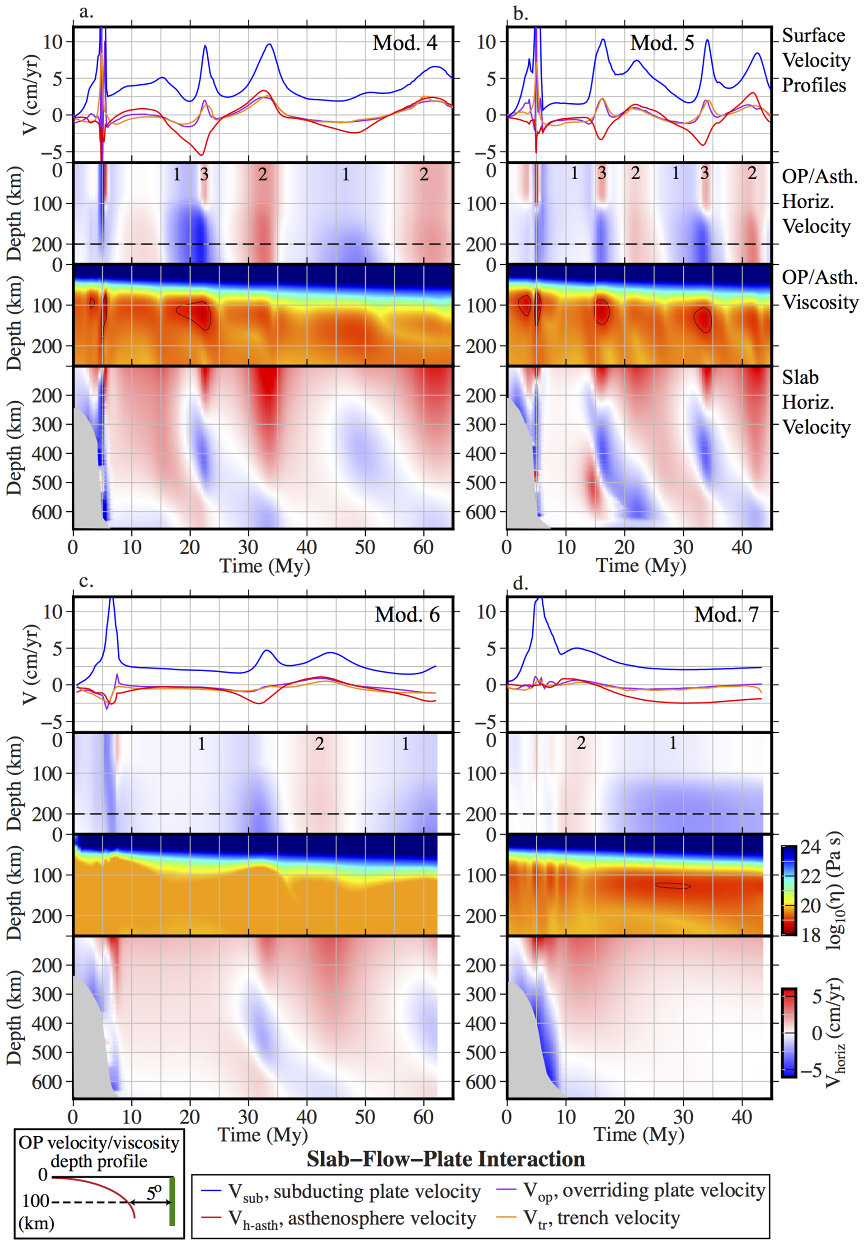

Figure 5: Effect of non-linear rheology on the coupling of slab, asthenosphere and plate flow. a–d) Models 4–7. Model 4 – reference case, model 5 – younger subducting plate, model 6 – $\eta_{min} = 5 \times 10^{19}$ Pa s, model 7 – no phase transitions. Top: velocity profiles versus time. Positive velocity is away from the trench/slab. Negative velocity is toward the trench/slab. V_{h-asth} is the longitudinal (horizontal) component of flow in the asthenosphere at a depth of 200 km taken from the vertical profile located 5 degrees from the top of the slab-surface at 100 km depth (see green line in schematic). Numbers refer to mode 1–3 slab-flow-plate interaction. Middle-top: vertical profile of longitudinal (horizontal) component of flow versus time. Middle-bottom: vertical profile of viscosity versus time (same location as V_{h-asth} profile). Black contour outlines times when the viscosity decreases to $\leq 10^{19}$ Pa s. Bottom: vertical profile (100–660 km depth) of the horizontal component of slab velocity versus time. The values are found by locating the point in the slab ($T < 1000°$C) with the maximum velocity magnitude at each depth.

3.2. Time-Dependent Thermal Structure

The episodic dynamics of the slab, plate and trench motion directly effects the time-dependent thermal structure of the subducting slab and the mantle wedge (Fig. 6). First, we find that the slab surface temperature (SST) depth profiles at a single time are quite similar to that found for steady-state kinematic wedge flow thermal models with similar parameters. The SST profiles are characterized by slow cooling of the slab at shallow depth, followed by rapid heating at the depth where the slab first comes into contact with hot mantle wedge material. In our models, this depth is primarily controlled by the basalt-to-eclogite transition, which determines the depth at which the crustal rheology is modeled to transition to that of olivine, but it also depends strongly on the minimum viscosity of the mantle. (This is similar in concept to case T550 from Syracuse et al. (2010) which modeled the partial-full coupling depth to occur when the slab surface temperature reached 550°C.)

For example, a model with relatively steady-state dynamics (model 7, no PT) has a thermal structure that is also uniform in time (Fig. 6a, i). Rapid heating occurs at 65–75 km depth with SSTs increasing from 300 to 750°C from 80 to 100 km depth, but then only reaching to 900°C at 250 km. During a brief period (5–7 my) of faster subduction, which advects cold isotherms to greater depth, SSTs are colder by 75 °C at 100 km, but are substantially colder (almost 250°C) at 75 km depth. However, after this time, there is little variation in the thermal profile as the slab dynamics are relatively steady. Interestingly even though this model has a relatively old slab (80 my), because it is subducting slowly (only 2.5 cm/yr), the SSTs predict melting of hydrated basalt over a narrow depth range (Fig. 6i).

In contrast, models with episodic slab folding exhibit substantially more variation in SSTs that primarily vary with the speed of the subducting plate (Fig. 6b, c). The hottest temperatures (up +225°C relative to the median temperature) occur early on during a period of very slow subduction immediately after the slab enters the lower mantle: at these times melting of the slab crust is predicted. The effect of slab age can be seen in slightly hotter SSTs for model 5 (40 my) compared to model 4 (80 my), but this is a smaller effect than variations in subduction rate from 2 to 15 cm/yr. During folding events the slab sinks rapidly (5–10 cm/yr) and SSTs drop by up to 250°C (at 100 km). These cold pulses can be followed along the slab surface to depths greater than 250 km and are reflective of much colder temperatures throughout the slab interior (see crust-mantle-boundary (CMB) profiles in Fig. 6i–l).

In addition to the coupling depth, the mantle viscosity has a strong effect on SSTs. In model 6, the higher minimum mantle viscosity causes the mantle wedge corner to deepen over time and this also shifts rapid heating of the slab surface from 75 km down to 100 km depth (Fig. 6d). Similar to model 7, because there is little variation in subduction rate, the SST profile is relatively constant in time. Also the median SST (deeper than the decoupling depth) is higher because the subduction rate is slower on average. At shallow depths, there is a slight shift to colder temperatures after 35 my coinciding with a shift to larger slab curvature (smaller slab dip) and growth of the accretionary prism above the shallower slab (see Fig. 4j–l).

Mantle wedge temperature is also affected by the minimum mantle viscosity, through the effect on shallow slab shape, rate of mantle flow into the wedge corner, and growth of the accretionary wedge. In models with a minimum viscosity of 10^{18} Pa s, flow in the mantle wedge corner is consistently shallower, predicting melting as shallow as 35

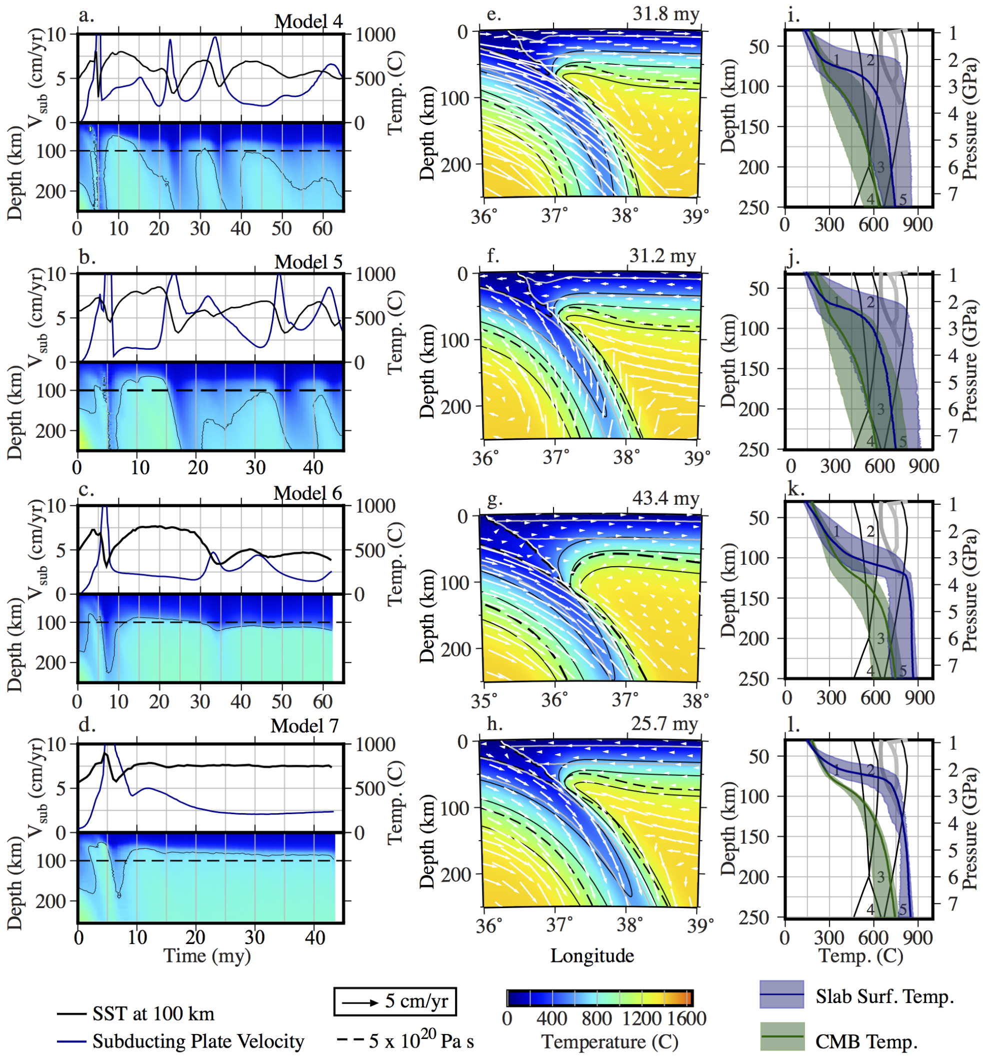

Figure 6: Time-evolution of slab-surface temperature (SST). Rows: 1–4 are Models 4–7. a–d) Bottom: temperature (color) along slab surface (depth) versus time. Black contour: 700 °C (temperature of wet basalt solidus at ≈ 80 km depth). Top: subduction velocity (blue) and SST at 100-km depth (black). Location of slab surface profile is shown in Fig. 1b and follows the crust contour. e–h) temperature in the slab and mantle wedge corner at times specified. Contours are the same as in Figure 4 with addition of a viscosity contour (dashed line). i–l) SST (blue) and crust-mantle boundary (CMB) temperature versus depth/pressure. Solid line: median temperature. Shading: range of minimum and maximum temperature. Dark/light gray lines are the solidi for wet/dry basalt (Vielzeuf and Schmidt, 2001). Black lines separating regions 1–5 are dehydration reaction for hydrated harzburgite (Hacker et al., 2003a): dehydration of serpentine/chlorite/brucite (1: 14.8% water), serpentine/chlorite dunite (2: 6.2 wt% water), chlorite/harzburgite (3: 1.4 wt% water), phase A (4: 6.8 wt% water), and dry garnet harzburgite (5).

km for wet peridotite and times when dry melting is possible (e.g., model 4; Fig. 7a, c). Note, the vertical profile is located where the slab-surface crosses 100 km depth. In contrast, when the minimum viscosity of the mantle is increased to 5×10^{19} Pa s, there is slow cooling of the mantle as the slab curvature increases from ≈ 200 km to ≈ 400 km (model 6, 10–30 my; Fig. 7b, d). This is followed by a more rapid increase in slab curvature from ≈ 400 km to

≈ 600 km (40–45 my) and a shift from hot mantle wedge conditions to a cold mantle wedge. In the cold state, even wet melting of peridotite is not possible along this profile (but could occur along vertical profiles locate further down the slab surface). However, even in the ”hot” mantle state, the wedge profiles are cooler by ≈ 100°C (Fig. 7b) compared to the models with a lower minimum mantle viscosity. In kinematic wedge thermal models, the mantle viscosity can be changed independent of slab geometry; these fully-dynamic models demonstrate that these parameters are not in fact independent and can lead to pronounced changes in slab-wedge thermal structure when there is self-consistent time-dependent evolution of slab geometry.

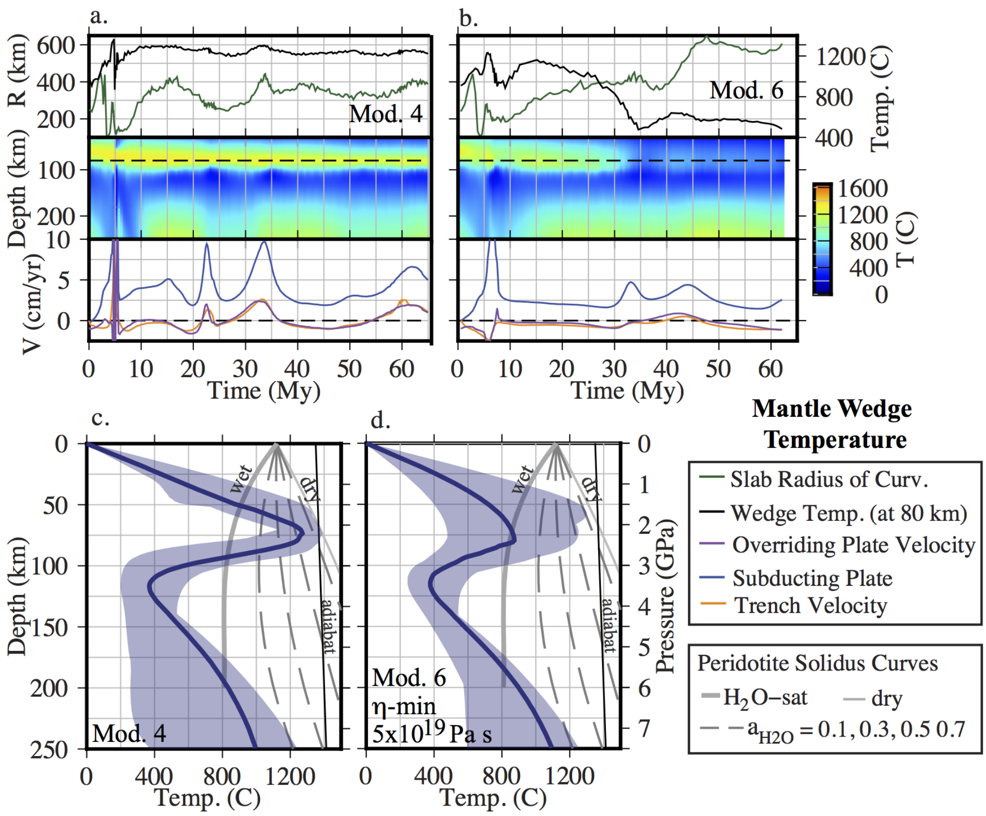

Figure 7: Time-evolution of mantle wedge temperature. a, c) Model 4. b, d) Model 6. a–b) Top: comparison of mantle wedge temperature at 80 km depth (black) to the radius of curvature of the slab (green: larger R indicates shallower dip). Middle: vertical profile of mantle wedge temperature versus time. Location of mantle wedge profile is shown in Fig. 1b. Bottom: plate and trench motion (see legend). c–d) Mantle wedge temperature versus depth/pressure. Dark blue: median temperature. Light blue shading: range of minimum and maximum temperature. Gray lines are the solidi (see legend) for wet to dry peridotite (Hirschmann, 2000; Till et al., 2010).

4. Discussion

Determining the relationship between plate and trench motion, and slab deformation is important for determining the key physical processes that govern coupling of large-scale mantle convection and plate tectonics (Conrad and

Lithgow-Bertelloni, 2002; Gérault et al., 2012). From the comparison of the plate motions at the surface, the asthenosphere flow and viscosity and the slab motion at depth, we find that there are three modes of slab-flow-plate interaction in the models:

Mode 1 (coupled retreat) occurs when the motion of the slab is primarily vertical sinking. In this case, slab sinking pulls the asthenosphere flow beneath the overriding plate toward the slab and the overriding plate is dragged toward the trench.

Mode 2 (coupled-advance) occurs when there is a large component of forward (prograde) motion of the slab along most of its length in the upper mantle. In this case, the prograde motion of the slab drives the asthenosphere flow away from the subducting slab, which also drags the overriding plate away from the trench. In all cases, there is also a horizontal component of forward motion across the shear zone pushing the overriding plate. Only in the mode 1 case is this motion overcome by the opposing flow-induced drag on the overriding plate. The proportion of forward motion needed to cause mode 2 flow depends on the stress-induced weakening of the asthenosphere.

Mode 3 (decoupled advance) occurs during initial stages of folding when the slab has a large component of prograde (positive) horizontal motion at shallow depths, while at deeper depths there is a large retrograde (negative) horizontal component. If the stresses induced by folding of the slab (seen as larger sinking rates) are large enough, then the non-linear weakening of the asthenosphere allows this prograde shallow motion to push the OP into advance, while the deeper retrograde motion pulls the underlying asthenosphere toward the slab.

There are three aspects of the physical model that combine to cause the three modes of slab-flow-plate intereaction. The first aspect is the slab rheology, including both the total stiffness (integrated strength across its thickness) and the plastic yielding under large stress. The large stiffness of the slab is a result of the strong-temperature dependence of the olivine viscosity, a large yield stress (1 GPa) used to mimic Peierls creep at high stress (Billen and Hirth, 2007) and a maximum viscosity cut-off of 10^{24} Pa s. The large stiffness leads to a significant component of prograde horizontal motion of the slab compared to a less stiff slab because the slab is strong enough to support its own weight when the bottom of the slab is supported by higher viscosity in the lower mantle. This effect can be seen by comparing V_{horiz}^{slab} for an older, stiffer slab (Model 4) and a younger, less stiff slab (Model 5): the older slab has larger V_{horiz}^{slab} that extend to deeper depths. The plastic yielding of the slab is also important because it allows the slab to weaken and localize deformation under large stresses: this allows the folding to occur even though the rest of the slab remains strong.

The second aspect is the compositionally-dependent phase transition (CDPT) model. Compared to simpler parameterizations of the phase transitions (e.g., olivine only with only two phase transitions), this more earth-like model provides less buoyancy-resistance at 660-km because of the counteracting effect of the pyroxene phase transitions at this depth. This difference is important because the slab is able to sink into the lower mantle and therefore it also creates a large return flow that includes the lower mantle: if the slab stagnates at the base of the transition, the return flow is isolated in the upper mantle and must drive more horizontal flow to balance the same amount of slab sinking in the upper mantle. The CDPT model also leads to a more distributed increase in the density of the slab starting at 410-km down through 520-km. A model with a the same density anomaly located only at the 410-km would tend to steepen the shallow slab (same force applied at shorter distance leads to more torque). This effect is demonstrated by the test model with olivine-only phase transitions: the slab stops sinking when it reaches 660-km and the stress transferred to the slab above 410-km is sufficient to cause the slab to break.

Finally, the third key aspect of the model that is the slab-induced, non-linear weakening of the mantle. The slab density is the main source of stress (e.g., besides ridge push) driving flow in the model. The viscosity structure controls how this stress is distributed (instantaneously) across the fluid, roughly decreasing exponentially with distance. However, when the viscosity is stress-dependent, this same stress can be accommodated at higher strain-rate leading to a lower effective viscosity. Because the non-linear viscosity also depends on temperature and increases with depth, the weakening response occurs primarily directly next to the slab and in the mantle wedge, where the stress is the highest. However, the weakening can also occur farther from the slab in the asthenosphere, because at shallow mantle depths and mantle temperatures the strain-rate accommodated by the dislocation creep (non-linear) is significantly higher than for diffusion creep (linear). This difference in strain-rates gets smaller with depth because the dislocation creep mechanism has a larger activation volume (viscosity increases faster with depth).

The significant impact of non-linear viscosity on slab dynamics and its ability to decouple mantle and plate flow direction has also been noted in instantaneous regional subduction models (Jadamec and Billen, 2010) and models of LPO (lattice-preferred orientation) development during the early stages of subduction (Jadamec, 2016; MacDougall et al., 2017). In addition, because changes to the strength of non-linearity (approximated in our models by limiting the minimum viscosity) affects trench motion and the subducting plate speed in the models, it may be possible to use these observations, together with other constraints on slab geometry, to better constrain lateral viscosity variations and absolute viscosity of the asthenosphere. For example, while model 6, does a better job of generating trench retreat, the maximum subducting plate speed is only 2.6 cm/yr, far below the maximum subducting plate speeds observed in the present-day (Lallemand et al., 2005). Therefore, the viscosity structure would need to change in such a way as to allow for faster subducting plate speeds, and more trench retreat. In particular, the models presented here assume uniform grain-size, do not include the effects of variations in water content (e.g., a wetter mantle wedge) or presence of melt, and use the same flow law for all the major compositions (except basalt). Thus, these model results provide the motivation for future studies that can systematically test the effects of more comprehensive rheological models, with a suite of observations that are sensitive to different parameters.

These results also present new challenges to applying an analytical force-balance approach to understanding how slabs drive plate motions. First, rather than ignoring the overriding plate in force-balance calculations (Capitanio, 2013), it must be considered in the analysis because slab-induced mantle flow affects the motion of the overriding plate and the resulting force works across the shallow plate interface to affect trench motion. During coupled phases, when the mantle flow pulls the overriding plate toward the trench it helps to prevent trench advance and drive trench retreat, whereas in decoupled phases, even though the asthenosphere flows toward the trench the overriding plate can be pushed by the advancing subducting plate. The ability of the overriding plate to affect trench motion has been demonstrated in other studies, for example, using a similar model set-up and non-linear rheology, but limiting the minimum viscosity to 10^{19} Pa s (Čížková and Bina, 2013). This conclusion is also supported by instantaneous models of subduction in a 2D cylindrical geometry with linear viscosity, which showed that the ability of strong slabs to drive trench advance is increased when there is a weak asthenosphere beneath the overriding plate (Gérault et al., 2012): that study concluded that this was because the weak asthenosphere partially decouples the plate and mantle and emphasizes the interaction between adjacent plates.

Second, rather than assessing the instantaneous force balance given a specified slab geometry, it is necessary to take into account how the evolving slab-induced stresses on the mantle can change the mantle viscosity structure. Both this study and the study by Jadamec (2016) show that the viscosity can be reduced by 10–100x, not just immediately around the slab, but reaching 500–1000 km from the slab beneath the plates. The models presented here show that these changes in viscosity structure can be rapid, and are happening continuously. However, the largest changes in viscosity in the models, those leading to complete decoupling of plate motion direction, are short-lived and relate to large changes in slab geometry, suggesting that such events may also be less common in the Earth (e.g., the time-scale of folding found in the models: 25–50 my). For example, if such a weakening event is necessary to allow for trench advance, than this could be one reason why trench advance is less prevalent in present-day observations of trench motion. More generally, however, other processes besides slab folding could also lead to weakening in the asthenosphere.

Analysis of the shallow thermal structure is in general agreement with the slab surface and mantle wedge temperatures predicted by kinematic-slab wedge-flow thermal models (Wada et al., 2008; Syracuse et al., 2010): thermal structure is primarily controlled by subduction rate, with secondary effects due to slab age and moderate changes in slab dip. However, unlike kinematic models there is a feedback between the evolving temperature and viscosity structure and the slab geometry. In particular, limiting the minimum viscosity within the mantle wedge causes the overriding plate to be dragged down into the mantle creating a broad, cold mantle wedge corner. While similar structures sometimes appear in published subduction models, the dynamic effects and the implications for melting in the mantle wedge (Elkins-Tanton et al., 2001; Kelemen et al., 2003; Cagnioncle et al., 2007; England and Katz, 2010), are not commonly addressed. Our results show, that the shallow wedge thermal structure is another important constraint on the upper mantle rheology. For example, from the behavior of model 6, it can be argued that if the effect of non-linear viscosity is generally more limited in the upper mantle, the wedge viscosity is probably kept weaker by the effects of water and/or melt (Billen and Gurnis, 2001; Arcay, 2017).

The models presented here also highlight the degree to which slab thermal structure can vary in response to changes in slab sinking rate. First, slab sinking rates vary from 2 to > 10 cm/yr in response to changing slab geometry during folding, buckling and recovery of the slab in the transition. Such long-term variation ins the subduction rate (25–50 my) could contribute to the long-term cyclical patterns observed in arc magmatism (Haschke et al., 2002;

DeCelles et al., 2009). In particular, most of the models predict possible melting of basaltic crust at the surface of the slab during periods of very slow subduction (< 2 cm/yr). However, they also predict substantial drops in SST during periods of fast subduction (5–10 cm/yr), which could severely limit dehydration of the slab (van Keken et al., 2002), loss of other volatiles (e.g., carbon Dasgupta and Hirschmann, 2010), and water-induced melting in the mantle wedge (Schmidt and Poli, 1998; Till et al., 2010, 2012). These results also show that the amount of water retained in slabs sinking deeper into the mantle could be highly variable. Such variability in water content could impact intermediate depth seismicity in the slab (Hacker et al., 2003b; Omori et al., 2004), release of water in the transition zone (Richard et al., 2007; Leahy and Bercovici, 2007; Myhill et al., 2017) and transport of water into the lower mantle (Hirschmann, 2006).

The model analysis highlights how the differences between the model design used in our studies and that used by other research groups has lead to the different slab dynamics, and plate and trench motions. The next question is then, how relevant are these models to understanding slab dynamics and plate motions in the Earth. As of yet, neither our models, nor other existing model do a satisfactory job of self-consistently matching the suite of observations characterizing slab dynamics and plate motion on Earth: the variation in slab shape reflecting differences in time-dependent deformation, correlations between slab shape, density, sinking rates, and subduction duration, the range of plate speeds, the relationship between different directions and rates of trench motion and slab deformation, and the thermal structure of the shallow slab and mantle wedge. And, we know of several simplifications that are likely to affect the ability of a model to reproduce not just a couple, but all of these observations. Most important amongst these simplifications for our models are: 1) the use of a 2D rather than 3D domain, 2) a model domain with sidewalls rather than a full sphere, 3) multiple surface plates and slabs and 4) a passive, lower mantle lacking density structures and thermal boundary conditions that would lead to both large-scale and small-scale upwelling.

However, we suggest that the models presented here bring us closer to earth-like subduction for several reasons. First, the models use an earth-like non-linear rheology, which is known to be active in the upper mantle, and which we have now shown plays a fundamental role in the coupling of plate-flow-slab interactions. Models that do not include non-linear rheology may be able to match some observations, but they tend to have very cold mantle wedges. More studies on the effect of non-linear rheology are necessary to better capture and understand the variables that control slab deformation: e.g., grain-size, Peierls creep versus a yield criterion, effects of water and melt in the mantle wedge. Second, we use the CDPT, which better represents an earth-like density distribution in the slab. Many studies have clearly shown that slab buoyancy is a fundamental control on slab dynamics and trench motion (Schellart, 2008b; Stegman et al., 2010; Ribe, 2010): therefore, using an earth-like density distribution and not just an averaged density is necessary to apply model results to slab dynamics on Earth. Third, our models produce both retreating and advancing trench motion with rates of about 1–2 cm/yr, and plate velocities in the range of 1–15 cm/yr after the slab reaches the lower mantle, in agreement with present-day observaitons. However, the models do not exhibit steady, longer term trench retreat or fast trench retreat rates. Therefore, further analysis are needed to understand how these other modes of slab-flow-plate interaction are achieved in models with more earth-like rheology and phase transitions. Fourth, our models produce folded slabs that sink slowly into the lower mantle, in agreement with the interpretation of many thick slab anomalies in the lower mantle (van der Hilst et al., 1997; Ritsema et al., 2004; Fukao et al., 2009; Simmons et al., 2015). Finally, the models presented here have slab and mantle wedge thermal structure that are consistent with previous kinematic thermal models that match a variety of temperature-related observations (e.g., dehydration, melting, surface heat flow). This is further evidence that the non-linear rheology, which is a key factor controlling the slab-wedge thermal structure, through its effect on the slab sinking rates and mantle flow rates, is a first order feature of an earth-like model of a subduction zone.

5. Conclusions

Using 2D fully dynamic models of subduction we have shown that there is a feedback between slab deformation and stress-induced weakening of the asthenosphere underlying the overriding plate through non-linear rheology. We find that there are three modes of interaction between the slab deformation, mantle flow and overriding plate motion. In mode 1 and mode 2 the overriding plate and underlying mantle have coupled motion with either trench retreat or advance, respectively. In mode 3, weakening of the asthenosphere allows the mantle to flow toward the retrograde motion of the folding slab, while the overriding plate is pushed by prograde advancing motion of the shallow slab and subducting plate. This kind of dynamically-controlled viscous resistance in the upper mantle complicates force-balance analysis of trench and plate motion, but also highlights the fact that the overriding plate is not passive and can help to drive trench retreat or advance (coupled) or allow rapid trench advance (decoupled). In addition, we find that modifying the overriding plate structure to include the ridge push force and crustal buoyancy leads to more trench retreat. However, because of the decoupling effects of the rheology and the effects of compositionally-dependent phase transitions on slab density, trench motion oscillates in response to slab folding without net trench retreat over time. Therefore, we conclude that the effects of non-linear rheology may be less-pronounced in the Earth's upper mantle in order to match observations of trench retreat. However, non-linear viscosity also affects the subducting plate speed and thermal structure in the mantle wedge. Therefore, reducing the effects of the non-linear rheology could also have the unwanted effect of producing plate speeds that are too slow and a mantle wedge that can not produce melts.Therefore, an increase in asthenosphere viscosity beneath the overriding plate should be added to models, while still allowing the mantle to weaken around the slab and in the mantle wedge. Finally, the episodic sinking rate of the slab causes significant time variability in thermal structure of the shallow slab system predicting periods of reduced volatile-induced melting in the mantle wedge and increased transport of volatiles to the transition zone and deep mantle.

Acknowledgements

This research was funded by the National Science Foundation, award #1246864. We thank Roberto Agrusta and an anonymous reviewer for their constructive and critical reviews. Billen acknowledges support from the Alexander von

Humboldt Foundation. The authors acknowledge the support of CIG in maintaining the CitcomS software package and GMT 5.0 for figure preparation.

References

Agrusta, R., Goes, S., van Hunen, J., 2017. Subducting-slab transition-zone interaction: Stagnation, penetration and mode switches. Earth and Planetary Science Letters 464, 10–23.

Alisic, L., Gurnis, M., Stadler, G., Burstedde, C., Wilcox, L. C., Ghattas, O., 2010. Slab stress and strain rate constraining global mantle flow. Geophysical Research Letters 32 (L22308).

Arcay, D., 2017. Modelling the interplate domain in thermo-mechanical simulations of subduction: Critical effects of resolution and rheology, and consequences on wet mantle melting. Physics of the Earth and Planetary Interiors 269, 112–132.

Arredondo, K., Billen, M. I., 2016. The effects of phase transitions and compositional layering in two-dimensional kinematic models of subduction. Journal of Geodynamics 100, 159–174.

Arredondo, K. M., Billen, M. I., 2017. Coupled effects of phase transitions and rheology in 2D dynamical models of subduction. Journal of Geophysical Research 122, 5813–5830.

Arrial, P.-A., Billen, M. I., 2013. Influence of geometry and eclogitization on oceanic plateau subduction. Earth and Planetary Science Letters 363, 34–43.

Billen, M. I., 2001. I. Seafloor morphology of the Osbourn Trough and Kermadec Trench and ii. Multiscale dynamics of subduction zones. Ph.D. Thesis, California Institute of Technology.

Billen, M. I., 2008. Modeling the dynamics of subducting slabs. Annual Reviews of Earth and Planetary Science 36, 325–356.

Billen, M. I., 2017. Insights into the causes of arc rifting from 2D dynamic models of subduction. Geophysical Research Letters 44, 1–10.

Billen, M. I., Gurnis, M., 2001. A low viscosity wedge in subduction zones. Earth and Planet. Sci. Lett. 193, 227–236.

Billen, M. I., Hirth, G., 2007. Rheologic controls on slab dynamics. Geochemistry, Geophysics and Geosystems 8 (Q08012).

Cagnioncle, A.-M., Parmentier, E. M., Elkins-Tanton, L. T., 2007. Effect of solid flow above a subducting slab on water distribution and melting at convergent plate boundaries. Journal of Geophysical Research 112 (B09402), 1–19.

Capitanio, F., Morra, G., Goes, S., 2007. Dynamic models of down-going plate-buoyancy driven subduction: Subduction motions and energy dissipation. Earth and Planetary Science Letters 262, 284–297.

Capitanio, F. A., 2013. Lithospheric-age control on the migrations of oceanic convergent margins. Tectonophysics 593, 193–200.

Christensen, U. R., 1996. The influence of trench migration on slab penetration into the lower mantle. Earth and Planet. Sci. Lett. 140, 27–39.

Christensen, U. R., Yuen, D. A., 1985. Layered convection induced by phase transitions. Journal of Geophysical Research 90 (B12), 10291–10300.

Cížková, H., Bina, C., 2013. Effects of mantle and subduction-interface rheologies on slab stagnation and trench rollback. Earth and Planetary Science Letters 379, 95–103.

Cížková, H., van Hunen, J., van den Berg, A. P., 2007. Stress distribution within subducting slabs and their deformation in the transition zone. Physics of the Earth and Planetary Interiors 161, 202–214.

Conrad, C. P., Lithgow-Bertelloni, C., 2002. How mantle slabs drive plate tectonics. Science 298, 207–209.

Currie, C. A., Wang, K., Hyndman, R. D., He, J., 2004. The thermal effects of steady-state slab-driven mantle flow above a subducting plate: the Cascadia subduction zone and backarc. Earth and Planetary Science Letters 223, 35–48.

Dasgupta, R., Hirschmann, M. M., 2010. The deep carbon cycle and melting in Earth's interior. Earth and Planetary Science Letters 298, 1–13.

DeCelles, P. G., Ducea, M. N., Kapp, P., Zandt, G., 2009. Cyclicity in Cordilleran orogenic systems. Nature Geoscience 2, 251–257.

Elkins-Tanton, L. T., Grove, T. L., Donnelly-Nolan, J., 2001. Hot shallow mantle melting under the Cascades Volcanic Arc. Geology 29, 631–634.

England, P. C., Katz, R. F., 2010. Melting above the anhydrous solidus controls the location of volcanic arcs. Nature 467 (700-704).

Forsyth, D., Uyeda, S., 1975. On the relative importance of the driving forces of plate motion. Geophysical Journal of the Royal Astronomical Society 43, 163–200.

Fukao, Y., Obayashi, M., Nakakuki, T., the Deep Slab Project Group, 2009. Stagnant slab: A review. Annual Reviews of Earth and Planetary Science 37, 19–46.

Funiciello, F., Faccenna, C., Heuret, A., Lallemand, S., Di Giuseppe, E., Becker, T. W., 2008. Trench migration, net rotation and slab-mantle coupling. Earth and Planetary Science Letters 271, 233–240.

Garel, F., Goes, S., Davies, D. R., Davies, J. H., Kramer, S. C., Wilson, C. R., 2014. Interaction of subducted slabs with the mantle transition-zone: A regime diagram from 2-D thermo-mechanical models with a mobile trench and an overriding plate. Geochemistry, Geophysics, Geosystems 15, 1739–1765.

Gérault, M., Becker, T. W., Kaus, B. J. P., Faccenna, C., Moresi, L. N., Husson, L., 2012. The role of slabs and oceanic plate geometry in the net rotation of the lithosphere, trench motions and slab return flow. Geochemistry, Geophysics, Geosystems 13 (4), Q04001.

Hacker, B. R., Abers, G. A., Peacock, S. M., 2003a. Subduction factory 1: Theoretical mineralogy, density, seismic wave speeds and H_2O contents. Journal of Geophysical Research 108 (B1, 2029).

Hacker, B. R., Peacock, S. M., Abers, G. A., Holloway, S. D., 2003b. Subduction factory 2: Are intermediate-depth earthquakes in subducting slabs linked to metamorphic dehydration reactions? Journal of Geophysical Research 108 (B1), 1–16.

Haschke, M., Siebel, W., Günther, A., Scheuber, E., 2002. Repeated crustal thickening and recycling during the Andean orogeny in north Chile (20°–26°s). Journal of Geophysical Research 107 (B1,2019).

Heuret, A., Lallemand, S. E., 2005. Plate motions, slab dynamics and back-arc deformation. Physics of Earth and Planetary Interiors 149, 31–51.

Hirschmann, M., 2000. Mantle solidus: experimental constraints and the effects of peridotite composition. Geochemistry, Geophysics and Geosystems 1 (2000GC000070), 1–26.

Hirschmann, M. M., 2006. Water, melting and the deep earth H_2O cycle. Annual Review Earth and Planetary Science 34, 629–653.

Hirth, G., Kohlstedt, D., 2003. Rheology of the upper mantle and the mantle wedge: a view from the experimentalists. In: Eiler, J. (Ed.), Inside the Subduction Factory. American Geophysical Union, Washington D.C.

Holt, A. F., Becker, T. W., 2017. The effect of a power-law mantle viscosity on trench retreat rate. Geophysical Journal International 208, 491–507.

Holt, A. F., Becker, T. W., Buffett, B. A., 2015. Trench migration and overriding plate stress in dynamic subduction models. Geophysical Journal International 201, 172–192.

Ita, J., King, S. D., 1994. Sensitivity of convection with an endothermic phase change to the form of governing equations, initial conditions, boundary conditions and equation of state. J. of Geophys. Res. 99 (B8), 15919–15938.

Jadamec, M. A., 2016. Slab-driven mantle weakening and rapid mantle flow. In: Morra, G. (Ed.), Subduction Dynamics: From Mantle Flow to Mega Disasters. Geophysical Monograph Series. John Wiley, Hoboken, N. J., pp. 135–155.

Jadamec, M. A., Billen, M. I., 2010. Reconciling surface plate motions with rapid three-dimensional mantle flow around a slab edge. Nature 465, 338–341.

Kelemen, P. B., Rilling, J. L., Parmentier, E. M., Mehl, L., Hacker, B. R., 2003. Thermal structure due to solid-state flow in the mantle wedge beneath arcs. In: Eiler, J. (Ed.), Subduction Factory, AGU Monograph. American Geophysical Union, pp. 1–19.

Lallemand, S., Heuret, A., Faccenna, C., Funiciello, F., 2008. Subduction dynamics as revealed by trench migration. Tectonics 27 (TC3014).

Lallemand, S. E., Heuret, A., Boutelier, D., September 2005. On the relationships between slab dip, back-arc stress, upper plate absolute motion and crustal nature in subduction zones. Geochemistry, Geophysics and Geosystems 6 (9), Q09006.

Leahy, G. M., Bercovici, D., 2007. On the dynamics of a hydrous melt layer above the transition zone. J. of Geophys. Res. 112 (B07401), doi:10.1029/2006JB004631.

Lee, C., King, S. D., 2011. Dynamic buckling of subducting slabs reconciles geological and geophysical observations. Earth and Planetary Science Letters 312, 360–370.

Lithgow-Bertelloni, C., Richards, M. A., 1998. The Dynamics of Cenozoic and Mesozoic plate motions. Reviews of Geophysics 36, 27–78.

MacDougall, J. G., Jadamec, M. A., Fischer, K. M., 2017. The zone of influence of the subducting slab in the asthenospheric mantle. Journal of Geophysical Research 122, 6599–6624.

McNamara, A. K., Zhong, S., 2004. Thermochemical structures within a spherical mantle: Superplumes or piles? Journal of Geophysical Research

109 (B07402).

Myhill, R., Frost, D. J., Novella, D., 2017. Hydrous melting and partitioning in and above the mantle transition zone: Insights from water-rich $MgO–SiO_2–H_2O$ experiments. Geochimica et Cosmochimica Acta 200 (408-421).

Omori, S., Komabayashi, T., Maruyama, S., 2004. Dehydration and earthquakes in the subducting slab: empirical link in intermediate and deep seismic zones. Physics of Earth and Planetary Interiors 146, 297–311.

Peacock, S. M., Wang, K., 1999. Seismic consequences of warm versus cool subduction metamorphism: examples from Southwest and Northeast Japan. Science 286, 937–939.

Quinteros, J., Sobolev, S. V., Popov, A. A., 2010. Viscosity in transition zone and lower mantle: Implications for slab penetration. Geophysical Research Letters 37, 1–5.

Ribe, N., Stutzmann, E., Ren, Y., van der Hilst, R., 2007. Buckling instabilities of subducted lithosphere beneath the transition zone. Earth and Planetary Science Letters 254, 173–179.

Ribe, N. M., 2010. Bending mechanics and mode selection in free subduction: a thin-sheet analysis. Geophys. J. Int. 180, 559–576.

Richard, G., Monnereau, M., Rabinowicz, M., 2007. Slab dehydration and fluid migration at the base of the upper mantle: implications for deep earthquake mechanisms. Geophysical Journal International 168, 1291–1304.

Ritsema, J., van Heijst, H., Woodhouse, J. H., 2004. Global transition zone tomography. Journal of Geophysical Research 109 (B02302).

Royden, L. H., Husson, L., 2006. Trench motion, slab geometry and viscous stresses in subduction systems. Geophysical Journal International 167 (881-905).

Schellart, W., 2008a. Subduction zone trench migration: Slab driven or overriding-plate-driven? Physics of Earth and Planetary Interiors 170, 73–88.

Schellart, W., Stegman, D., Farrington, R., Moresi, L., 2011. Influence of lateral slab edge distance on plate velocity, trench velocity, and subduction partitioning. J. of Geophys. Res. 116 (B10408).

Schellart, W. P., 2004. Quantifying the net slab pull force as a driving mechanism for plate tectonics. Geophysical Research Letters 31 (L07611).

Schellart, W. P., 2008b. Kinematics and flow patterns in deep mantle and upper mantle subduction models: Influence of the mantle depth and slab to mantle viscosity ratio. Geochemistry, Geophysics and Geosystems (G^3) 9 (3).

Schellart, W. P., Freeman, J., Stegman, D. R., Moresi, L., May, D., 2007. Evolution and diversity of subduction zones controlled by slab width. Nature 446.

Schellart, W. P., Stegman, D. R., Freeman, J., 2008. Global trench migration velocities and slab migration induced upper mantle volume fluxes: Constraints to find an Earth reference frame based on minimizing viscous dissipation. Earth-Science Reviews 88, 118–144.

Schmidt, M. W., Poli, S., 1998. Experimentally based water budgets for dehydrating slabs and consequences for arc magma generation. Earth and Planet. Sci. Lett. 163, 361–379.

Sdrolias, M., Müller, R. D., 2006. Controls on back-arc basin formation. Geochemistry, Geophysics and Geosystems 7 (4), Q04016.

Simmons, N. A., Myers, S. C., Johannesson, G., Matzel, E., Grand, S. P., 2015. Evidence for long-lived subduction of an ancient plate beneath the southern Indian ocean. Geophysical Research Letters 42, 1–9.

Stadler, G., Gurnis, M., Burstedde, C., Wilcox, L. C., Alisic, L., Ghattas, O., 2010. The dynamics of plate tectonics and mantle flow: from local to global scales. Science 329, 1033–1037.

Stegman, D., Farrington, R., Capitanio, F., Schellart, W., 2010. A regime diagram for subduction styles from 3-D numerical models of free subduction. Tectonophysics 483, 29–45.

Stegman, D. R., Freeman, J., Schellart, W. P., Moresi, L., May, D., 2006. Influence of trench width on subduction hinge retreat rates in 3-D models of slab rollback. Geochemistry, Geophysics and Geosystems 7 (3), Q03012.

Stein, C. A., Stein, S. A., 1992. A model for the global variation in oceanic depth and heat flow with lithospheric age. Nature 359 (123-129).

Syracuse, E. M., van Keken, P. E., Abers, G. A., 2010. The global range of subduction zone thermal models. Physics of the Earth and Planetary Interiors 183, 73–90.

Tan, E., Choi, E., Thoutireddy, P., Gurnis, M., Aivazis, M., 2006. GeoFramework: Coupling multiple models of mantle convection within a computational framework. Geochemistry, Geophysics and Geosystems 7 (6), Q06001.

Till, C. B., Elkins-Tanton, L. T., Fischer, K. M., 2010. A mechanism for low-extent melts at the lithosphere-asthenosphere boundary. Geochemistry, Geophysics and Geosystems 11 (10), Q10015.

Till, C. B., Grove, T. L., Withers, A. C., 2012. The beginnings of hydrous mantle wedge melting. Contributions to Mineralogy and Petrology 163, 669–688.

van der Hilst, R. D., Widiyantoro, S., Engdahl, E. R., 1997. Evidence for deep mantle circulation from global tomography. Nature 386, 578–584.

van Dinther, Y., Morra, G., Funiciello, F., Faccenna, C., 2010. Role of the overriding plate in the subduction process: Insights from numerical models. Tectonophysics 484, 74–86.

van Keken, P. E., Kiefer, B., Peacock, S. M., October 2002. High-resolution models of subduction zones: Implications for mineral dehydration reactions and the transport of water into the deep mantle. Geology, Geochemistry and Geophysics 3 (10), 1056, doi:10.1029/2001GC000256.

Vielzeuf, D., Schmidt, M. W., 2001. Melting relations in hydrous systems revisited: application to metapelites, metagraywackes and metabasalts. Contributions to Mineralogy and Petrology 141, 251–267.

Wada, I., Wang, K., He, J., Hyndman, R. D., 2008. Weakening of the subduction interface and its effects on surface heat flow, slab dehydration, and mantle wedge serpentinization. Journal of Geophysical Research 113 (B04402).

Yoshida, M., 2017. Trench dynamics: Effects of dynamically migrating trench on subducting slab morphology and characteristics of subduction zones systems. Physics of the Earth and Planetary Interiors 268, 35–53.

Zhong, S., Zuber, M. T., Moresi, L., Gurnis, M., 2000. Role of temperature-dependent viscosity and surface plates in spherical shell models of mantle convection. J. of Geophys. Res. 105, 11063–11082.